nature communications

Article

https://doi.org/10.1038/s41467-025-57311-w

Synthesis of high quality two dimensional covalent organic frameworks through a self-sacrificing guest strategy

Received: 10 September 2024

Accepted: 13 February 2025

Published online: 27 February 2025

Check for updates

Tianwei Xue[1], Li Peng[1] ✉, Chengbin Liu[1], Ruiqing Li[1], Rongxing Qiu[1], Yunyang Qian[2], Xinyu Guan[2], Shanshan Shi[1], Guangkuo Xu[1], Lilin Zhu[1], Shuliang Yang[3] ✉, Jun Li[1] ✉ & Hai-Long Jiang[2] ✉

The quality of covalent organic frameworks (COFs) crucially influences their mechanistic research and subsequent practical implementations. However, it has been widely observed that the structure damage induced by the activation procedure could compromise the quality of COFs. Here we develop a self-sacrificing guest method for synthesizing high-quality two-dimensional COFs (SG-COFs) by incorporating salt guests into the pores of the COF structure. These introduced salts play an indispensable role in supporting COF pores and mitigating quality loss during the activation process. Interestingly, due to the unique characteristic of salts decomposing into gases upon heating, this method can ultimately enable the synthesis of highly pure, high-quality COFs without the presence of residual guest molecules. The resulting sixteen COFs display superior crystallinity and porosity compared to those synthesized using conventional routes. Moreover, these high-quality SG-COFs have demonstrated to be highly efficient adsorbents for removal of per- and poly-fluoroalkyl substances.

As a fascinating class of crystalline polymer network, covalent organic frameworks (COFs) consist of ordered and periodic structures interlinked by covalent bonds[1,2]. Because of the ordered nanopores, high surface areas, crystallinity, and stability, COFs hold great promise in various novel applications, including catalysis[3,4], separation[5], adsorption[6], sensing[7], electrochemistry[8,9], gas storage[10], etc. Generally, the material quality could greatly affect its practical applications[11]. For instance, the importance of accessible porosity in processes like adsorption or separation has been substantiated, since the blocked pores and amorphous structure may impede effective mass transfer[12]. Further, potential applications in catalysis and electrochemistry require high degree of crystallinity and ordered stacking to improve electron separation and facilitate efficient electron transport[13]. Two-dimensional COFs (2D COFs) have received considerable attention, in which the planar arrangements with long-range order stack along the z-axis to form three-dimensional macromolecule assemblies[14]. The stacked sheets provide sufficient open-oriented apertures for selective substance transport and storage, while the conjugated planar layers contribute to the formation of crystalline structures[15,16].

Currently, researches on 2D COFs primarily focus on their topological structures, new linkage formation, covalent bond properties, and synthesis methods. However, the impact of structure damage caused by activation, which is common in 2D COFs and has significant effects on their structure and applications, has been rarely reported. For a long time, it has been commonly presumed that the majority of 2D COFs exhibit characteristics of rigid porous crystals[17]. Nevertheless, recent years have witnessed an increasing body of evidence suggesting that the structure of some COFs are not completely robust[18–23]. Owing to the weak noncovalent interactions both between and within layers, including π-π effects[20], electrostatic interactions[24], hydrogen

[1]College of Chemistry and Chemical Engineering, Xiamen University, Xiamen, Fujian 361005, China. [2]Hefei National Research Center for Physical Sciences at the Microscale, Department of Chemistry, University of Science and Technology of China, Hefei, Anhui 230026, China. [3]College of Energy, Xiamen University, Xiamen, Fujian 361102, China. ✉e-mail: li.peng@xmu.edu.cn; ysl@xmu.edu.cn; junnyxm@xmu.edu.cn; jianglab@ustc.edu.cn

bonding[25], etc, many COFs exhibit a certain degree of flexibility. Some of them are even considered fragile, indicating that they may not endure certain stresses or conditions in their potential applications.

Indeed, many 2D COFs have been found to be sensitive to the activation processes, resulting in diminished porosity and unsatisfactory crystallinity after solvent exchange/removal (Fig. 1a). For example, Dichtel et al. demonstrated that certain 2D COFs with imine links were prone to damage upon isolation and activation through vacuum drying[18]. Moreover, Yaghi and co-workers discovered that the flexible COF-117 maintained its crystallinity through solvent treatment but lost it upon activation[26]. In addition, Media's group showed that some 2D COFs underwent disorder and porosity lose when exposed to solvents or solvent vapors, due to the weak π-π interactions between adjacent layers[19]. Usually, the synthesis of COF materials involves solvent exchange and activation process to achieve dry, porous materials suitable for subsequent applications. During the activation, removing the solvent from the pores could give rise to the formation of amorphous materials with inferior crystallinity and low surface area. This phenomenon arises from capillary forces exerted during evaporation within nanoscale spaces[27], ultimately resulting in structural distortions and the collapse of pores. The sensitivity of COFs to activation processes could even lead to misinterpreted conclusions regarding the success of crystallization. More significantly, these characteristics impose severe limitations on their various practical applications, such as adsorption and separation processes.

Although the material quality loss triggered by the activation process is occasionally noted in the literature, there are limited reports on how to address this issue. Reducing capillary stress generated during solvent removal by employing gentler activation methods, such as supercritical carbon dioxide ($ScCO_2$) drying, is a viable strategy for preserving the pores of porous materials[19,28]. We also reported that $ScCO_2$ could facilitate synthesis of robust imine-linked 2D COFs[29]. However, $ScCO_2$ method necessarily requires specialized equipment and technology due to the high pressures involved, which is not universally available and can be potentially dangerous in various scenarios. Actually, there is a possible alternative approach to resolve this issue, which is to enhance the bearing capacity of COF channels. By filling the channels with robust substance, just like a vascular stent, the reinforced pore may have the potential to withstand structural distortions and resist pore collapse during activation. The introduction of guest molecules, such as polymers, to enhance stability in metal-organic framework materials has been reported[29–31]. Nonetheless, we have noticed that the guest molecules in these literatures are notoriously difficult to be completely removed, which will severely hamper the restoration of the original clear COF structures. This persistent presence of guest residues would essentially and potentially impede the research and application of the pristine COFs.

In this work, we present a straightforward and safe strategy, termed "self-sacrificing guest (SG) method", for the synthesis of high-quality 2D COFs. This method only requires two simple steps: impregnation and crystallization (Fig. 1b). To prevent the structure of COFs from collapsing during activation, decomposable salt molecules are introduced as guest molecules into the unactivated COF pores by ion impregnation and anti-solvent recrystallization. The salt guests filling the pores serve as a robust support, effectively mitigating or eliminating capillary stress induced by solvent removal. More interestingly, due to the characteristic of salts decomposing into gases upon heating, they are also removed during the activation process without causing pore damage. Finally, the activated COF material with high crystallinity and surface area could be easily obtained. By eliminating the need for high-pressure gas and specialized equipment, this method ensures safety, cleanliness, economy, green, and simplicity.

To systematically and comprehensively evaluate the generality of this approach, we report the preparation of ten imine-linked 2D COFs, one urea-linked 2D COF, one hydrazone-linked 2D COF, one hydrazine-linked 2D COF, one vinylene-linked 2D COF, one imide-linked 2D COF, and one keto-enamine linked 2D COF by the SG method (SG-COFs-1 ~ 16) (Fig. 2). All the SG-COFs consistently show superior crystallinity and higher surface area compared to those COFs prepared via conventional route (Con-COFs-1 ~ 16). These positive results underscore the effectiveness of the SG method in mitigating material quality loss, a common dilemma encountered in the synthesis of 2D COFs. Furthermore, we demonstrate these high-quality SG-COFs exhibit distinctly enhanced functional performance in removing per- and polyfluoroalkyl substances from complex water matrices.

Results

Strategy development, synthesis and characterization

To verify our hypothesis regarding the applicability of the SG method for high-quality COF synthesis, we selected a prototypical 2D COF

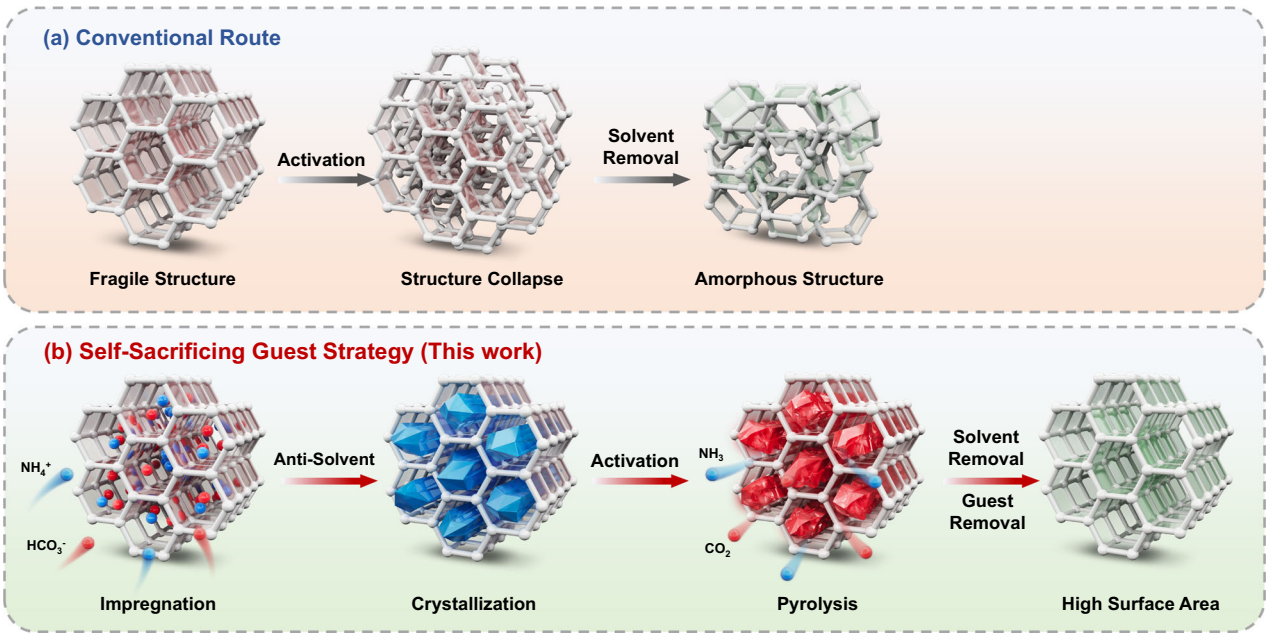

Fig. 1 | Schematic illustration. Illustration showing activated COFs synthesized by **a** conventional route and **b** SG strategy.

https://doi.org/10.1038/s41467-025-57311-w

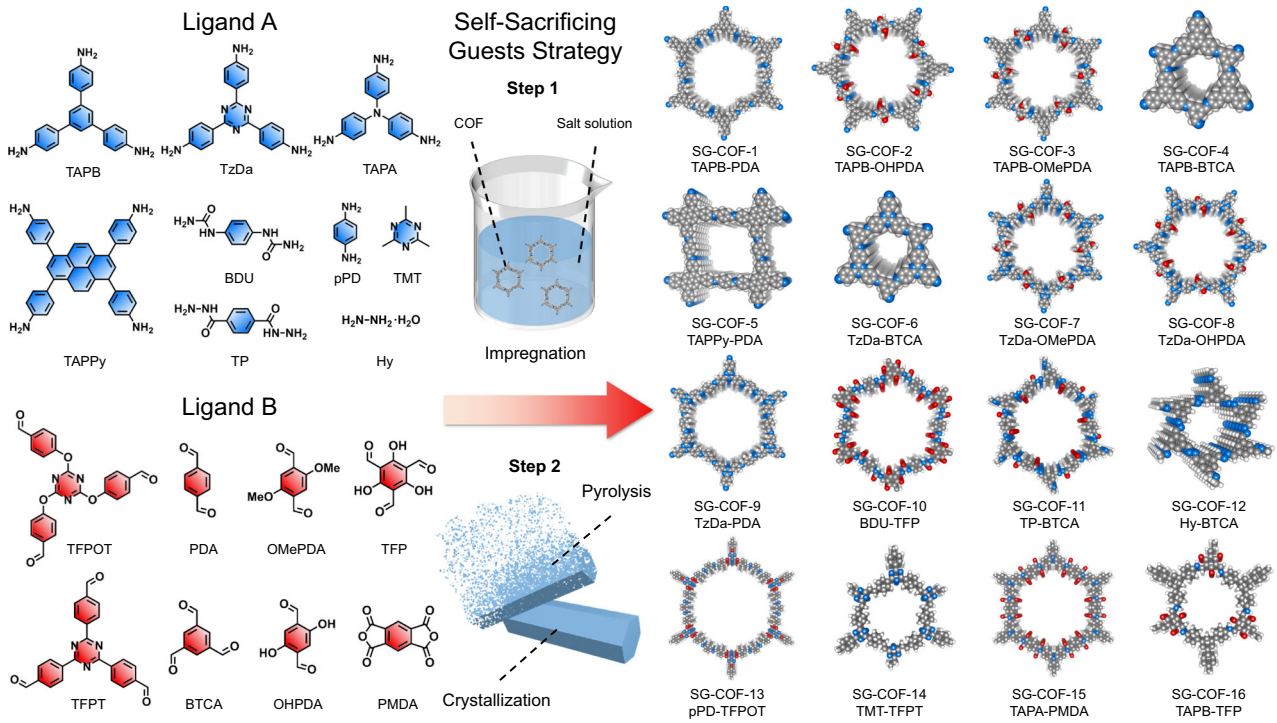

Fig. 2 | Apparatus and conditions used for SG strategy, the COFs studied and the monomers used to synthesize them. The monomers (left) and structures (right) of sixteen COFs prepared by the SG strategy (center).

known as TAPB-PDA COF (COF-1). This COF is formed by the condensation of 1,3,5-tris(4-aminophenyl)benzene (TAPB) and terephthalaldehyde (PDA) (Fig. 3a), which has been extensively studied for its synthesis, activation and formation mechanism[23,32]. It is worth noting that this COF is widely recognized to be sensitive to activation processes[18,33]. First, for the synthesis of TAPB-PDA COF by the conventional method (denoted as Con-COF-1), it was synthesized at 70 °C for 72 h using γ-valerolactone (GVL) as the solvent, and 10.5 M aqueous acetic acid served as the catalyst. Then, the as-synthesized yellow solid was washed with methanol thoroughly and subsequently activated under vacuum at 100 °C overnight to obtain dry solid powder.

As shown in powder X-ray diffraction (PXRD) pattern (Fig. 3b), the activated Con-COF-1 exhibited minimal characteristic peaks, which indicated its weak crystallinity. According to the nitrogen adsorption and desorption isotherms at 77 K (Fig. 3c), Con-COF-1 presented a much lower specific surface area than expected, demonstrating the loss of porosity. These superficial results potentially distorted the accurate assessment of successful material synthesis, and made it difficult to draw precise conclusions about the underlying mechanisms from product analysis. In other words, the lack of crystallinity and porosity is not attributed to the absence of crystallization during COF polymerization, but rather by the damage of COF structures during activation. Due to the surface tension of the solvent, capillary stress is spontaneously generated when the solvent inside the pores becomes gaseous during the activation process, and the pore strength of many COFs cannot balance and resist this stress effect, ultimately leading to the partial or complete destruction of the pores[27]. This is not amorphous in the sense of crystallography[34]. Even if we attempted to replace the high-boiling point solvent (γ-valerolactone, b.p. 207 °C) needed for synthesis with a low-boiling point solvent (methanol, b.p. 65 °C) to reduce surface tension[35], it remained regrettably ineffective. It is worth mentioning that, mild $ScCO_2$ activation can yield high-quality COFs (Supplementary Fig. 4). However, $ScCO_2$ activation requires specialized high-pressure equipment and complex operations.

Therefore, it is necessary to explore a simple and effective method to address the issue of the material quality loss of COFs during activation, driven by the challenges posed by the surface tension and capillary stress. The crucial step is to improve the robustness of the COF pores by introducing suitable guest molecules that can stabilize the pores and enable them to be maintained during conventional activation processes, such as heating and vacuum conditions. Meanwhile, in order to obtain pure COFs, the guest molecules need to be easily and completely removed. After deep thinking, we were focusing on thermally decomposable salts, for example, ammonium bicarbonate (NH_4HCO_3). This salt is rarely used and is seldom considered a guest molecule due to its intrinsic instability, but we have effectively leveraged its decomposable properties in this pioneering study.

After COF polymerization, salt ions were easily introduced into COF pores through stirring and impregnating. Following this, the addition of a poor solvent (isopropanol) led to recrystallization of salt ions into salt crystals, effectively filling into COF pores. These solid crystals are robust enough to support the pores to resist capillary stress generated by solvent removal. Further, these NH_4HCO_3 salts could be directly decomposed into gas molecules (NH_3, CO_2, and H_2O) during activation. Based on classical physical chemistry theory, the surface tension during the direct transformation from solid to gas is much lower than that from liquid to gas, which is highly beneficial for pore preservation and preventing collapse[36,37]. Consequently, the pure high-quality COFs with high crystallinity and porosity could be obtained via the above method, which we named as SG method. Worth mentioning, by washing the decomposed waste gas with water, the NH_4HCO_3 salts can be easily recycled and reused, making the entire process highly green and sustainable, and with the potential for large-scale production[38,39]. It should be pointed out that although this method is similar to the freeze-drying process in principle, high-quality COFs could not be obtained by freeze drying (Supplementary Fig. 1), likely due to the structural damage stemming from the volume expansion (about 9%) of water into ice within the COF pores during the freezing process[33].

https://doi.org/10.1038/s41467-025-57311-w

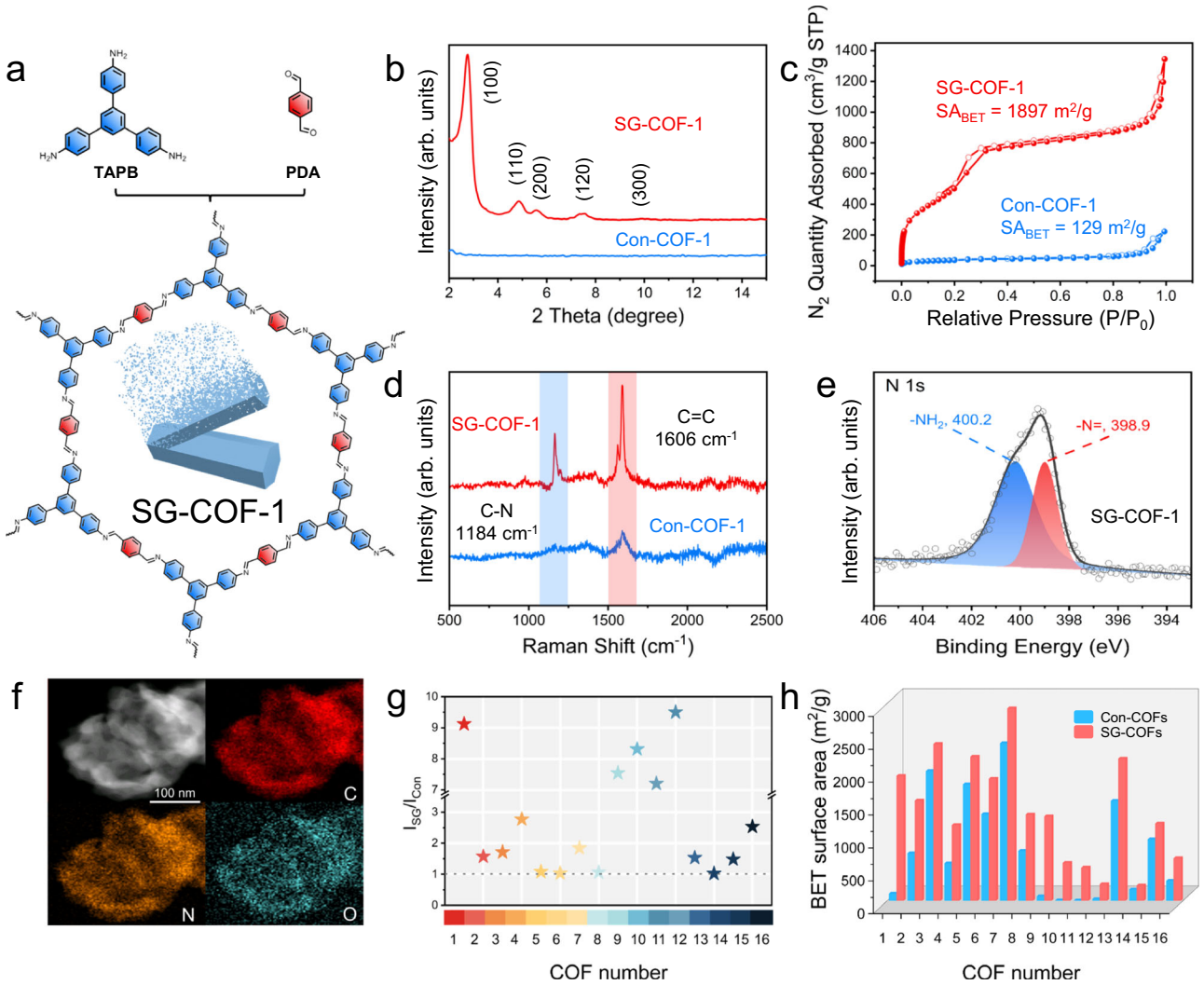

Fig. 3 | Characterizations of Con-COF-1 and SG-COF-1. a Synthesis route for SG-COF-1 (TAPB-PDA). **b** PXRD patterns, **c** N_2 adsorption and desorption isotherms at 77 K, and **d** Raman spectra of SG-COF-1 and Con-COF-1 after activation. **e** N 1 s X-ray photoelectron spectrum of SG-COF-1. **f** STEM image and energy-dispersive X-ray spectroscopy (EDX) elemental maps of SG-COF-1. **g** Comparison of the intensities of (100) diffraction peaks in PXRD patterns of SG-COFs and Con-COFs. **h** Comparison of the BET surface areas of SG-COFs (red) and Con-COFs (blue).

Bearing the above-mentioned points in mind, we utilized the SG method for the fabrication of TAPB-PDA COF, and subsequently, the resulting powder was subjected to methanol washing and thermal-vacuum activation (referred to as SG-COF-1). Completely different from Con-COF-1, the PXRD pattern of SG-COF-1 (Fig. 3b) displayed clearer and more distinct peaks at 2.8°, 4.9°, 5.7°, 7.5°, and 10°, respectively, corresponding to (100), (110), (200), (210), and (220) planes of typical TAPB-PDA COF (Supplementary Fig. 2). Furthermore, the N_2 adsorption and desorption experiments at 77 K (Fig. 3c and Supplementary 3) showed that SG-COF-1 had a high Brunauer-Emmett-Teller (BET) surface area (1897 m^2/g), which had increased by a factor of 15 compared with that of Con-COF-1 (129 m^2/g). This positive result indicated that SG-COF-1 retained a well-defined pore structure after activation. It is worth noting that, despite employing harsh conditions for activation, the vacuum-activated SG-COF-1 still presented a surface area comparable to that of $ScCO_2$ activated Con-COF-1, which required specialized high-pressurized equipment and technology (Supplementary Fig. 4). Additionally, the more distinct Raman peaks of SG-COF-1 versus the faint features of Con-COF-1[33,40] (Fig. 3d) manifested that SG-COF-1 preserved a more ordered crystal framework[41,42]. These characterizations clearly demonstrated that it was feasible to attain higher quality TAPB-PDA COF with enhanced crystallinity through the SG strategy.

Next, the high purity of SG-COF-1 was examined. The N 1 s X-ray photoelectron spectra showed that SG-COF-1 (Fig. 3e), displayed peaks at 400.2 and 398.9 eV, corresponding to -NH_2 and -N = , respectively[43]. These peaks, which are also present in TAPB-PDA COF, were consistent with those observed in the spectrum of Con-COF-1 (Supplementary Fig. 5). In the spectrum of SG-COF-1, there was no peak corresponding to NH_4^+ in NH_4HCO_3[44]. Moreover, 20 mg of as-synthesized SG-COF-1 was soaked in 10 mL of ultra-pure water for 24 h, and ion chromatography analysis of the supernatant suggested that there were no ammonium ions in the soaking solution (Supplementary Fig. 6). These results provided strong evidence that the salts were completely removed during the activation process. Further, no significant differences were observed in the solid state nuclear magnetic resonance spectroscopy (Supplementary Fig. 7) and Fourier transform infrared spectroscopy (Supplementary Fig. 8) of SG-COF-1 and Con-COF-1. These results indicated that the SG method did not alter the characteristic chemical bonds and intrinsic polymerization type of the original COF. Scanning electron microscope (SEM) images and transmission electron microscope (TEM) images (Fig. 3f, Supplementary Figs. 9 and 10) also displayed that the morphology of SG-COF-1 was similar to that of Con-COF-1, exhibiting the morphology of nanoparticles.

Moreover, the thermogravimetric analysis curves illustrated that SG-COF-1 exhibited similar thermal stability to Con-COF-1, further confirming the complete removal of salts from SG-COF-1 (Supplementary Fig. 11). Worth noting, we also found that the kinetics of TAPB-PDA COF formation could be obscured by the damage caused by activation process, as reported by Dichtel[18]. Actually, when the synthesis time was shortened from 72 h to 4 h, high-quality COF material could also be obtained through the SG method (Supplementary Fig. 12). These findings explicitly highlighted the advantage of the SG strategy in fabricating high-quality 2D COFs with ordered pore structures, as well as its effectiveness in deriving precise mechanistic insights from product analysis.

Mechanism studies

After successfully preparing high-quality COFs using the SG method, we became increasingly interested in how it worked detailedly behind its effectiveness. To clarify this, we focused on examining three crucial steps involving salts in this approach: recrystallization, supporting effect and thermal decomposition (Fig. 4a). First, salt ions were introduced into the pores of the synthesized COF without activation through the impregnation of NH_4HCO_3 salt solution. Afterwards, the introduction of anti-solvent changed the solubility and allowed the salt to recrystallize. Microscopic image and mass spectrometry imaging microscope image of SG-COF-1 without activation reflected the mixture of salt and COF (Supplementary Fig. 13). Compared with those of Con-COF-1, it could be clearly observed the formation of salt crystals in SG-COF-1 after recrystallization. Worth noting, shape measurement laser microscopy system indicated that the salts located outside the COF pores exhibited much larger size compared to those inside the COF pores (Fig. 4b and Supplementary Fig. 14). This phenomenon is reasonable and could be attributed to the nanoconfinement effect, which restricts nucleation and growth of NH_4HCO_3 crystals in the confined COF nanopores[45,46]. Due to the obstruction posed by the COF pore wall, salt crystals tend to preferentially grow along the less resistant one-dimensional pore direction, consequently filling the COF pores. Then, the rigid salt aids in supporting the pores during activation, preventing pore collapse induced by capillary stress arising from solvent removal. In detail, during the activation process, it is inevitable for pores to shrink, leading to the collapse of the microstructure and a decrease in surface area. This collapse of the microstructure is caused by capillary force, which is induced by the presence of liquid-gas interfaces in the pore spaces between the solid networks. When activation causes a reduction in liquid volume, the surface of the liquid will contract and create a curvature (with radius r), and the surface tension between the liquid and gas (P_{LV}) will create a shear stress, or capillary force (P_{cap}). The formula for P_{cap} is given by Eq. (1):

$$P_{cap} = \frac{2P_{LV}}{r} \tag{1}$$

With the transition from liquid to gas, the capillary force can reach 100–200 MPa in the pore channel[47]. However, in the case of SG-COF, the rigid salt crystals effectively support the pore channels, and this support counteracts and balances the capillary force, significantly reducing pore shrinkage and layer movement of COF, thereby preventing structural damage and preserving crystallinity and surface area. Additionally, during the thermal decomposition of the salt crystals, due to their rigidity, the solid-gas interface in the pore channels does not create a curved surface like a liquid-gas interface, and therefore, almost no capillary force is generated. Therefore, the removal of salts has negligible to no impact on the structure.

To verify this supporting effect, the dynamic structural transformations of Con-COF-1 and SG-COF-1 were tracked in real-time during the activation process. For this, the Con-COF-1 without activation was dispersed in suitable amount of isopropanol and the obtained dispersion was directly dropped onto the silica plate. Subsequently, PXRD tests were executed promptly and repeated every 3 min until the isopropanol was vaporized completely (Supplementary Fig. 15). Changes of the PXRD patterns reflected the transformation of the crystalline structure throughout the entire solvent removal process (Fig. 4c).

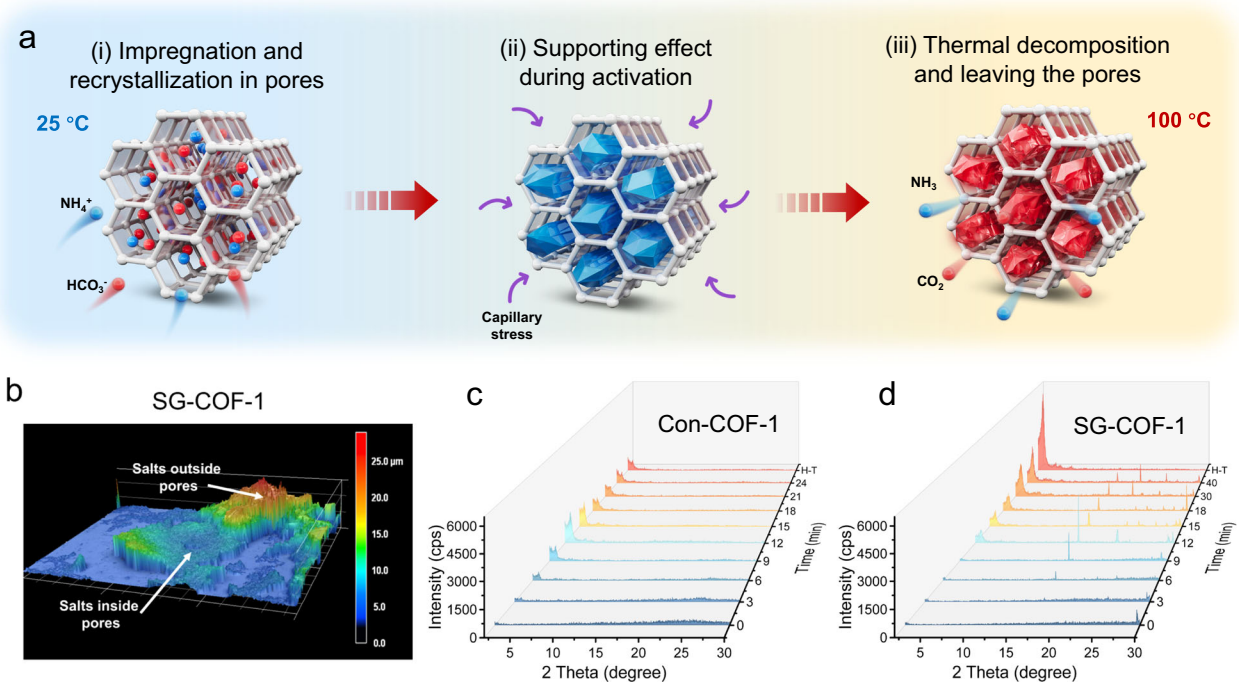

Fig. 4 | Mechanism studies. a Schematic illustration for three steps of the SG method. **b** Simulated 3D image of SG-COF-1 by shape measurement laser microscopy system. Intensity changes of PXRD peaks along with solvent volatilization for **c** Con-COF-1 and **d** SG-COF-1.

https://doi.org/10.1038/s41467-025-57311-w

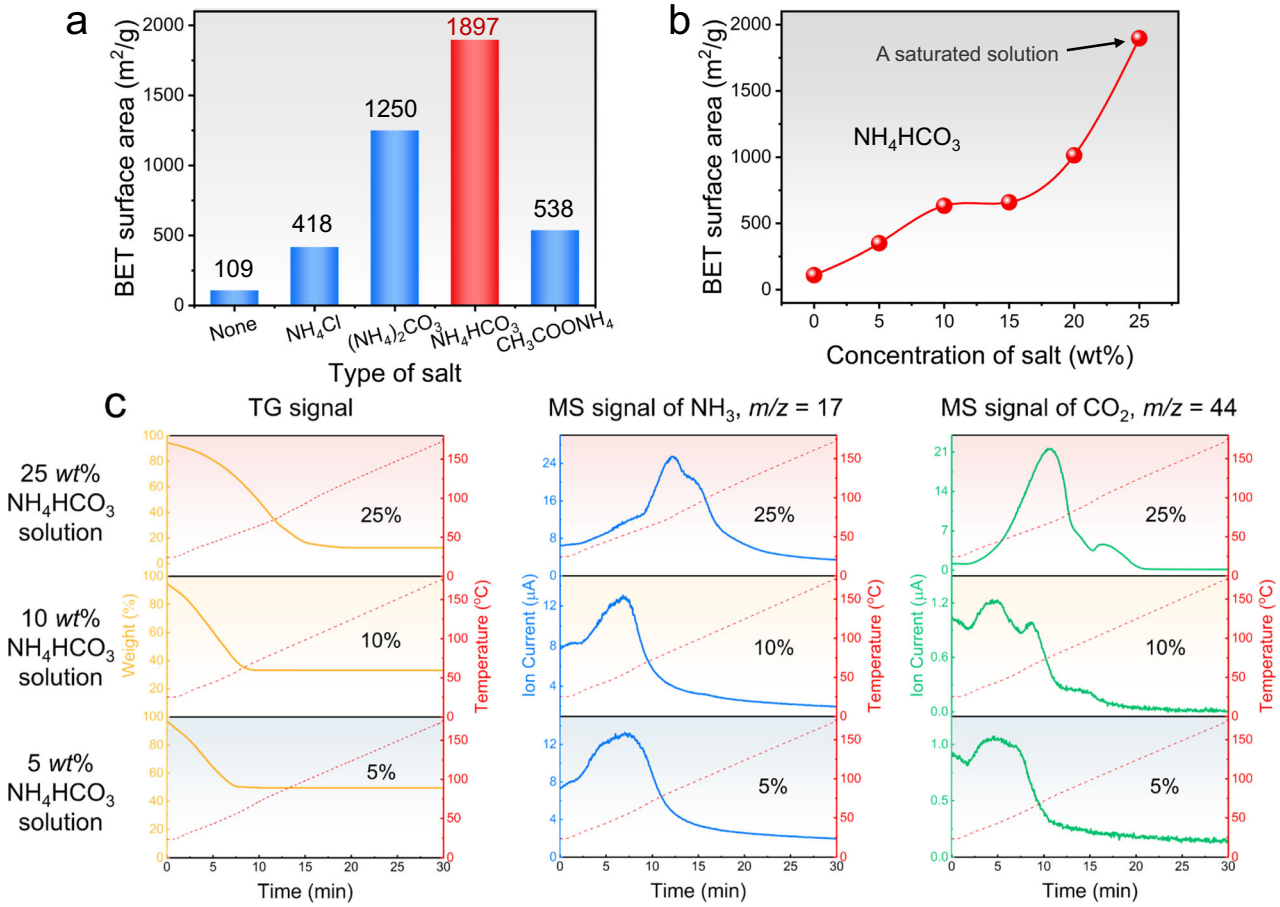

Fig. 5 | Studies on thermal decomposition of salts. a BET surface area of SG-COF-1 synthesized with different types of salts. **b** Optimization of the BET surface area for SG-COF-1 prepared using different concentrations of NH_4HCO_3. **c** Thermogravimetric curves and mass spectrometry curves of SG-COF-1 constructed by varied concentrations of NH_4HCO_3 during the activation process.

In the initial stage, the PXRD patterns displayed low peak intensity, attributed to the presence of numerous solvent molecules between the COF layers[17]. As the isopropanol molecules continuously volatilized, the crystalline attributes of COF gradually intensified. During this process, the incorporation of solvent molecules within the COF pores contributed to the stabilization of the framework. And then, as isopropanol further evaporated, the capillary force provoked by surface tension of solvent removal brought a certain damage to the COF structure, leading to a state of disorder. This rational analysis was substantiated by the gradual decline in peak intensity observed in the PXRD patterns. On the contrary, in the case of SG-COF-1, the presence of salt crystals supporting the COF pores displayed a continuous increase in the peak intensity of COF as the isopropanol continuously evaporated (Fig. 4d). Meanwhile, obvious characteristic peaks consistent with NH_4HCO_3 (the sharp peaks at 2theta values > 15°) could be observed. Furthermore, after heat treatment, the peaks of NH_4HCO_3 completely disappeared, while the (100) peak of the COF was further intensified upon losing the decomposable filler by thermal decomposition. These experimental results indicated that the surface tension associated with the direct transformation of solid NH_4HCO_3 to gas was negligible and did not cause structural damage to the COF pores.

Additionally, we thoroughly inspected the thermal decomposition properties of the salts during the activation process. Firstly, the influence of pyrolytic salts with different decomposition products on COF quality was analyzed. Various kinds of salts including NH_4Cl, $(NH_4)_2CO_3$, NH_4HCO_3 and CH_3COONH_4 (Supplementary Table 1) were individually introduced into the COF pores following the same impregnation and recrystallization process, and then these COFs were thermally activated afterwards. The N_2 adsorption and desorption experiments revealed that salts such as $(NH_4)_2CO_3$ and NH_4HCO_3 decomposed to produce NH_3, CO_2, and H_2O, which endowed COFs with a high surface area (Fig. 5a). In contrast, NH_4Cl and CH_3COONH_4, which decomposed to generate acids such as HCl and CH_3COOH, resulted in lower porosity. This reduced porosity is likely due to the disruptive effects of these acids on the COF structure.

We further investigated the effects of different concentrations of NH_4HCO_3 solutions on SG-COF-1. Gratifyingly, we observed that as the concentration increased, the BET surface area of the obtained COFs increased consistently until the NH_4HCO_3 solution was saturated (Fig. 5b). To inspect the reasons behind, real-time thermal decomposition process was tracked by directly conducting thermogravimetric analysis coupled with mass spectrometry on the material after recrystallization process (Fig. 5c). The mass spectrometry signals corresponding to NH_3 (*m/z*, 17) and CO_2 (*m/z*, 44) could be associated with the decomposition of NH_4HCO_3. Based on the analysis curves, in the case of low concentration, insufficient salt in the pores resulted in a fast decomposition rate, and nearly complete decomposition occurred in the early stage of activation. This rapid decomposition was unable to provide perfect supporting effect throughout the entire activation process. As a result, it led to a low surface area. With the concentration increased, the decomposition process was delayed, allowing the salt to stay within the COF pores for a longer period and effectively support the structure during the whole solvent removal process. Consequently, higher concentrations of the salt solution contributed to the synthesis of high-quality COFs.

Versatility of the SG strategy

To demonstrate the versatility of the SG strategy, we attempted to extent this method to synthesize a broader range of COFs, including ten imine-linked COFs, one hydrazone-linked COF, one hydrazine-linked COF, one urea-linked COF, one vinylene-linked COF, one imide-linked COF, and one keto-enamine linked COF. These COFs included: SG-COF-2, composed of TAPB and 2,5-dihydroxyterephthalaldehyde (OHPDA) (Supplementary Fig. 16); SG-COF-3, composed of TAPB and 2,5-dimethoxyterephthalaldehyde (OMePDA) (Supplementary Fig. 17); SG-COF-4, composed of TAPB and benzene-1,3,5-tricarbaldehyde (BTCA) (Supplementary Fig. 18); SG-COF-5, composed of 1,3,6,8-tetrakis(4-aminophenyl)pyrene (TAPPy) and PDA (Supplementary Fig. 19); SG-COF-6, composed of 4,4′,4″-(1,3,5-triazine-2,4,6-triyl)trianiline (TzDa) and BTCA (Supplementary Fig. 20); SG-COF-7, composed of TzDa and OMePDA (Supplementary Fig. 21); SG-COF-8, composed of TzDa and OHPDA (Supplementary Fig. 22); SG-COF-9, composed of TzDa and PDA (Supplementary Fig. 23); SG-COF-10, composed of 1,3,5-triformylphloroglucinol (TFP) and 1,4-phenylenediurea (BDU) (Supplementary Fig. 24); SG-COF-11, composed of BTCA and terephthalohydrazide (TP) (Supplementary Fig. 25); SG-COF-12, composed of BTCA and linear hydrazine (Hy) (Supplementary Fig. 26); SG-COF-13, composed of p-phenylenediamine (pPD) and 2,4,6-tris(4-formylphenoxy)-1,3,5-triazine (TFPOT) (Supplementary Fig. 27); SG-COF-14, composed of 2,4,6-trimethyl-1,3,5-triazine (TMT) and 2,4,6-tris(4-formyl-phenyl)-1,3,5-triazine (TFPT) (Supplementary Fig. 28); SG-COF-15, composed of tris(4-aminophenyl)amine (TAPA) and pyromellitic dianhydride (PMDA) (Supplementary Fig. 29); and SG-COF-16, composed of TAPB and TFP (Supplementary Fig. 30). For comparison, the aforementioned COFs were also synthesized using the conventional method (Con-COF-x, x = 2 ~ 16) as control. Significantly, the Con-COF-9, -10 and -11 were also reported to be frag ile, making it challenging to achieve high porosity after activations[17,26,48–50].

PXRD data was collected under identical conditions for both Con-COFs and SG-COFs for comparative analysis, and the patterns (Supplementary Figs. 16–26) showed that all SG-COFs exhibited higher crystallinity. Further, the ratio of I_{SG}/I_{Con} (Fig. 3g) reflected the comparison of the (100) peak intensities between Con-COFs and SG-COFs, where I_{SG} represented the intensity of the (100) peak for SG-COFs and I_{Con} denoted the intensity of the (100) peak for Con-COFs. We observed that all values of I_{SG}/I_{Con} were greater than one, demonstrating that SG-COFs possessed higher diffraction peak intensity than the Con-COF ones. The increase in intensity was attributed to the more ordered arrangement of crystal structures in SG-COFs. What is more, we use the estimated domain size as a metric for crystallinity[51]. Scherrer analysis conducted through the full-width at half-maximum (FWHM) of the (100) plane indicates that SG-COFs exhibit larger estimated domain sizes, implying fewer defects and higher crystallinity (Supplementary Table 6). Additionally, N_2 adsorption and desorption isotherms at 77 K (Supplementary Figs. 16–26) revealed that SG-COFs exhibited higher BET surface areas compared to Con-COFs (Fig. 3h). This finding confirmed that SG-COFs maintained a more porous structure successfully. Moreover, it is important to highlight that SG-COFs manifested BET surface areas that are either higher than or comparable to those reported in the literatures for similar COFs (Supplementary Table 2). These positive results clearly demonstrate that, despite the common issue of structural damage caused by activation in COF materials, the SG method is a proven and effective strategy for producing high-quality COFs with both high crystallinity and surface area. However, it should be pointed out that we found the SG strategy is not suitable for COFs that are intrinsically unstable in water, such as boronic ester COF, SG-COF-17, composed of 2,3,6,7,10,11-hexahydroxytriphenylene (HHTP) and 4,4′-biphenyldiboronic acid (BPDA) (Supplementary Fig. 31). Compared with Con-COF-17, this material completely loses its crystallinity due to its decomposition in water.

Removal performance of per- and polyfluoroalkyl substances

Given that high accessible porosity is a highly advantageous merit for adsorption performance[52,53], we conducted tests on both imine-linked Con-COFs and SG-COFs to evaluate their effectiveness in adsorbing toxic pollutants from water. The aim was to explore whether the high-quality COFs obtained through the SG method could provide additional benefits in later-stage practical applications. Known as “toxic time bomb” and “forever chemicals”, per- and polyfluoroalkyl substances (PFAS) have attracted much attention in recent years[54]. PFAS including perfluoroalkyl carboxylic acids (PFCAs), perfluoroalkyl sulfonic acids (PFSAs), hexafluoropropylene oxide dimer acid (GenX) and so on (Fig. 6a), are widely used in plastic processing and manufacturing processes. These chemicals are notoriously difficult to degrade and can continuously accumulate in the environment and human body[55]. Therefore, removing PFAS from water matrices is becoming an urgent priority.

Here, we tried to use the as-synthesized high-quality COFs as the efficient adsorbents for PFAS removal from water. On the one hand, the hydrophobic interactions between the hydrophobic framework of COFs and the hydrophobic C-F chains on the PFAS are beneficial for the instant adsorption of PFAS on COFs (Supplementary Fig. 32). On the other hand, the electrostatic interactions between the cationic amines of the COFs and the carboxylate or sulfonate headgroup of the anionic PFAS could also contribute to the adsorption process (Fig. 6b)[56].

Firstly, adsorption experiments were performed using 5 mg each of Con-COF-1 ~12 and SG-COF-1 ~ 12 as adsorbents, with perfluorooctanoic acid (PFOA), a typical PFAS, serving as the target compound. In 10 mL of PFOA solution with initial concentration of 2000 ppm, the adsorption capacity of SG-COFs was obviously higher than that of Con-COFs (Fig. 6c and Supplementary Table 3), which was consistent with the observed trends in surface area. The more ordered structure of SG-COFs could create a more hydrophobic environment within the frameworks, thereby enhancing the hydrophobic interactions. Additionally, the increased accessible and well-defined porosity could expose more functional groups in an ordered way, serving as the chemical and structural basis for PFAS recognition. Next, more detailed researches were conducted on Con-COF-1 and SG-COF-1. It could be found that SG-COF-1 demonstrated a much faster adsorption rate compared with Con-COF-1 (Fig. 6d). SG-COF-1 removed ~90% of PFOA in <2 min and over 99% of PFOA in 10 min. In stark contrast, Con-COF-1 removed only 85% of PFAS even after 2 h. These results suggest that the increased accessible porosity in SG-COF-1 significantly enhances mass transfer and accelerates the adsorption process. Considering that the presence of other organic micropollutants may also significantly affect the affinity of PFAS on adsorbents, the removal performance of SG-COF-1 was further assessed under the interference of 10 fold of humic acid (Fig. 6e). Remarkably, SG-COF-1 still removed over 99% of PFAS, reaffirming its high affinity for PFOA removal. After that, the regeneration ability of SG-COF-1 was explored using a mixed regeneration solution consisting of NaCl and methanol to restore the saturated SG-COF-1 (Fig. 6f). Methanol was used to weaken the hydrophobic interactions between the COF framework and the C-F chains on PFAS[57], and Cl^- could facilitate the desorption of PFAS from the amine groups to allowing them to re-dissolve in methanol[58]. After three cycles, SG-COF-1 still retained >90% of its initial adsorption capacity and after five cycles, over 80% was retained, demonstrating its effective regeneration ability.

Next, the performance of Con-COF-1 and SG-COF-1 was evaluated in several real water samples (Fig. 6g). Specifically, 0.5 ppm of PFOA was added into urban water from drain-pipe (Xiamen, China), industrial water from a fluorosilicon material production base (Zibo, China), the Yangtze River water (Nanjing, China), and East China Sea water (Xiamen, China). Following treatment with the adsorbents, SG-COF-1 showed a higher removal percentage than Con-COF-1 across all tested water matrices. This indicates that high-quality COFs synthesized by

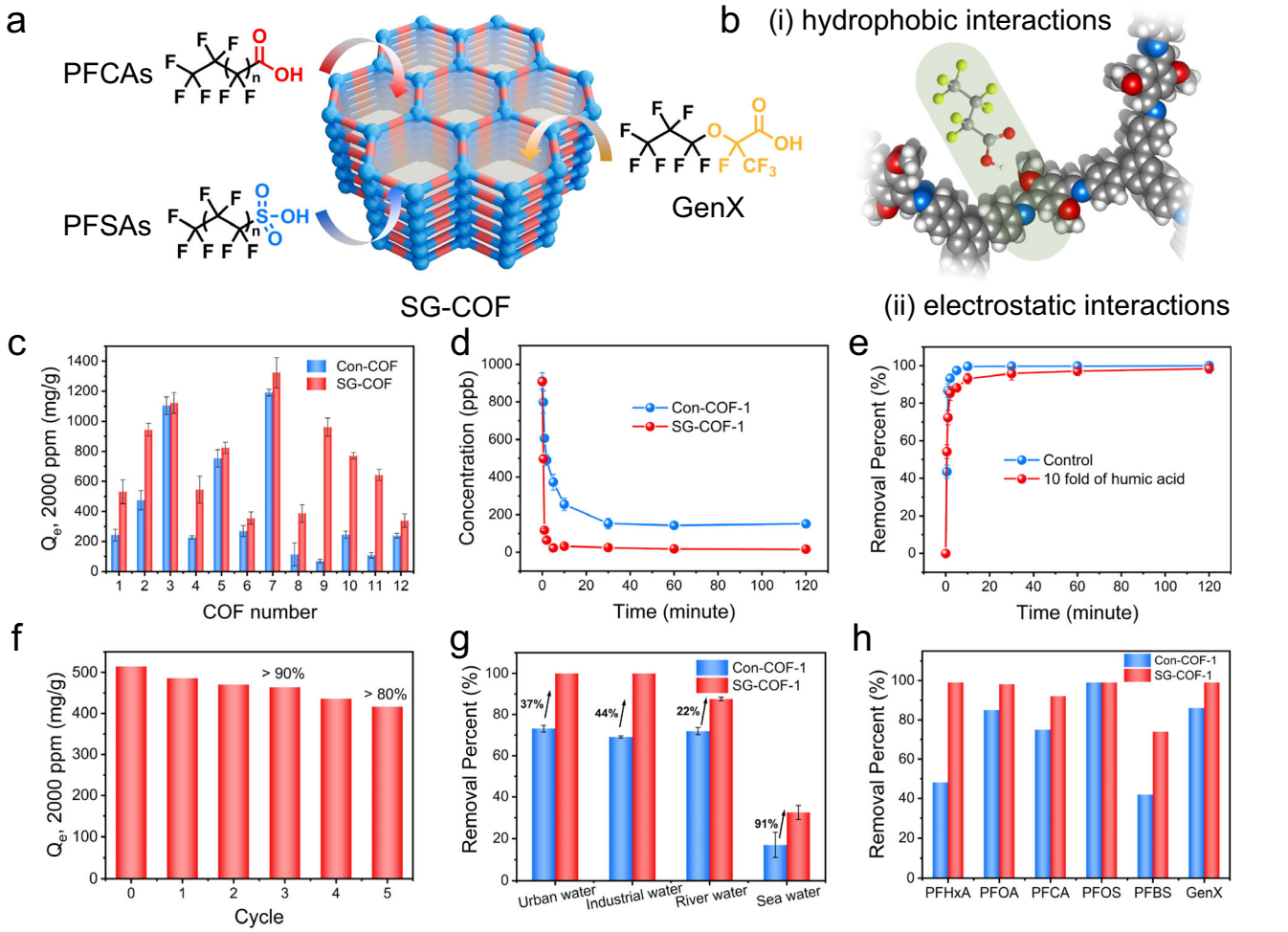

Fig. 6 | PFAS removal experiments of SG-COFs. a Schematic illustration for PFAS removal by SG-COFs. **b** Proposed adsorption mechanisms of PFAS on SG-COFs. **c** Adsorption capacity of PFOA by Con-COFs and SG-COFs at initial concentration of 2000 ppm. **d** Adsorption kinetics of PFOA by Con-COF-1 and SG-COF-1. **e** Removal efficiency of PFOA by SG-COF-1 under the interference of 10-fold of humic acid. **f** Evaluation of cyclability of SG-COF-1. **g** Removal efficiency of PFOA by Con-COF-1 and SG-COF-1 in different water matrices. **h** Removal efficiency of different PFAS by Con-COF-1 and SG-COF-1.

the SG strategy possess stronger practical application capabilities. Furthermore, we investigated the adsorption performances of Con-COF-1 and SG-COF-1 with six different PFAS compounds, including three types of PFCAs (PFHxA, PFOA, PFCA), two types of PFSAs (PFOS, PFBS), and GenX (Fig. 6h and Supplementary Table 4). For this analysis, 5 mg of each COF material was added to 10 mL of water samples spiked with ~1 ppm of different PFAS compounds. SG-COF-1 exhibited a broader and more comprehensive affinity for various PFAS compared to Con-COF-1. We should emphasize that, even in comparison with the reported adsorbents, SG-COF still demonstrates superior and more comprehensive PFAS removal capabilities (Supplementary Table 5).

Discussion

In summary, we have developed a simple, clean, green, sustainable and universal approach for synthesizing high-quality 2D COFs by introducing decomposable salts into the COF pores. The salts introduced through ion impregnation and anti-solvent recrystallization could fill the pores and serve as a robust support to mitigate the capillary stress caused by solvent removal. This intensification helps prevent the collapse of COFs during the subsequent activation stage. Interestingly, salts naturally decompose into gases upon mild heating, allowing them to be completely removed during the activation process. This design effectively eliminates the undesired interferences from guest molecules in COF research and applications. As a result, the activated COF materials with superior crystallinity and porosity could be easily obtained.

By employing this facile SG method, sixteen high-quality 2D COFs were successfully prepared and all these materials exhibited higher crystallinity and surface area compared to COFs synthesized by conventional methods. It is particularly impressive that the BET surface area of one of these COFs, SG-COF-1, increases by up to 15 times compared to the original COF. More importantly, the SG method enhances the functional properties of COFs, as demonstrated by the improved removal of PFAS from complex water matrices. The prepared SG-COFs exhibited higher adsorption capacity, faster removal rate, broader-spectrum affinity, and stronger practical application capabilities than the Con-COFs. It is anticipated that this safe, fast, green and economical method will have significant potential for the large-scale synthesis of various high-quality COFs, and this advancement could greatly expand their applicability for later-stage implementations.

Methods

Chemicals

Unless otherwise specified, all chemicals were used without further purification. 1,3,5-tris(4-aminophenyl)benzene (TAPB, 98%), terephthalaldehyde (PDA, 99%), 2,5-dimethoxyterephthalaldehyde (OMePDA, 98%), p-phenylenediamine (pPD) and 2,5-dihydroxyterephthalaldehyde (OHPDA, 97%) were purchased from Shanghai Meryer. Perfluorooctanoic acid (PFOA), 1,2,4-trichlorobenzene, perfluorooctane sulfonate (PFOS), perfluorohexanoic acid (PFHxA), perfluorocapric acid (PFCA) and 1,3,5-benzenetricarbaldehyde (BTCA,

98%) were bought from Sigma-Aldrich. 1,3,6,8-tetrakis(4-aminophenyl) pyrene (TAPPy), terephthalohydrazide (TP) and potassium perfluorobutanesulfonate (PFBS) were purchased from Aladdin. 1,4-dioxane, mesitylene, *o*-dichlorobenzene, 4,4′,4″-(1,3,5-triazine-2,4,6-triyl) trianiline (TzDa), γ-valerolactone, 1,3,5-triformylphloroglucinol (TFP) and 1,4-phenylenediurea (BDU) were purchased from Energy Chemical. Ammonium perfluoro(2-methyl-3-oxahexanoate) (GenX) was bought from AccuStandard. Isoquinoline, tris(4-aminophenyl)amine (TAPA), pyromellitic dianhydride (PMDA), 2,4,6-tris(4-formylphenoxy) -1,3,5-triazine (TFPOT), 2,4,6-trimethyl-1,3,5-triazine (TMT), 2,4,6-tris(4-formyl-phenyl)-1,3,5-triazine (TFPT), 2,3,6,7,10,11-hexahydroxytriphenylene (HHTP) and 4,4′-biphenyldiboronic acid (BPDA) were purchased from Acmec biochemical. Methanol, *N*-methyl-2-pyrrolidinone (NMP), tetrahydrofuran (THF), isopropanol, n-butanol, linear hydrazine (Hy), glacial acetic acid, ammonium bicarbonate, ammonium carbonate, ammonium chloride and ammonium acetate were provided by Sinopharm Chemical Reagent Co., Ltd. Deionized water was used throughout all experiments.

The urban water was collected in Xiamen, China (Xiamen, China, Latitude: 24.438357, Longitude: 118.094672, Collection Time: 2023.08.16). The industrial water was collected in Dongyue fluorosilicon material production base, Zibo, China (Zibo, China, Latitude: 36.973589, Longitude: 118.046506, Collection Time: 2023.10.02). The Yangtze river water was collected in Nanjing, China (Nanjing, China, Latitude: 32.156613, Longitude: 118.800723, Collection Time: 2021.03.21). The East China Sea water was collected in Xiamen, China (Xiamen, China, Latitude: 24.442217, Longitude: 118.075667, Collection Time: 2021.04.06).

Synthesis of SG-COFs

The as-synthesized COFs (The synthesis procedures can be found in the supplementary information) without activation were transferred to a centrifugal tube respectively and washed with methanol and water 3 times. Care was taken at this stage to prevent COF from drying in the centrifugal tube. Then the solid was dispersed in 15 mL of saturated ammonium bicarbonate solution and sonicated to uniform dispersion. Then the mixture was stirred for 4 h. After the specified time, the solid was isolated and 5 mL of isopropanol was added. Finally, the solid was subjected to vacuum activation at 100 °C.

Characterization

Powder X-ray diffraction was tested on Rigaku Ultima-IV X with a Cu Kα source (1.54056 Å) at 40 kV and 30 mA. All nitrogen adsorption and desorption were performed on an ASAP 2020 HD88 instrument. Scanning Electron Microscopy (SEM) characterizations were performed on ZEISS Sigma. Transmission Electron Microscopy (TEM) images were collected by JEM1400 and F30. Microscopic images, laser images and 3D images were collected by shape measurement laser microscopy system (VK-X250K). Mass spectrometry images were collected by imaging mass spectrometry microscope (iMScope QT). Raman spectra were collected using a Renishaw Invia instrument. The thermogravimetric analysis curve was obtained using TGA 449F5. The thermogravimetric curves and mass spectrometry curves were obtained by thermogravimetric analysis-mass spectrometry (SDT 650 and Discovery MS). Solid State Nuclear Magnetic Resonance (SSNMR) characterizations were performed on Bruker 400 MHz Avance III SS-NMR. X-ray photoelectron spectroscopy measurements were tested by Quantum 2000XPS with Omicron hemispherical energy analyzer. The quantitation of targeted PFAS was performed by the high-performance liquid chromatography system coupled with mass spectrometer (Shimadzu HPLC-MS 2020).

Data availability

All data generated or analyzed during this study are included in the Article and its Supplementary Information, and are available from the corresponding author upon request.

References

1. Côté, A. P. et al. Porous, crystalline, covalent organic frameworks. *Science* **310**, 1166–1170 (2005).
2. Geng, K. Y. et al. Covalent organic frameworks: design, synthesis, and functions. *Chem. Rev.* **120**, 8814–8933 (2020).
3. Zhang, J., Cheng, C., Guan, L. J., Jiang, H. L. & Jin, S. B. Rapid synthesis of covalent organic frameworks with a controlled morphology: an emulsion polymerization approach via the phase transfer catalysis mechanism. *J. Am. Chem. Soc.* **145**, 21974–21982 (2023).
4. Zou, H. B. et al. Amphiphilic covalent organic framework nanoparticles for pickering emulsion catalysis with size selectivity. *Angew. Chem. Int. Ed.* **63**, e202314650 (2024).
5. Wang, Z. F., Zhang, S. N., Chen, Y., Zhang, Z. J. & Ma, S. Q. Covalent organic frameworks for separation applications. *Chem. Soc. Rev.* **49**, 708–735 (2020).
6. Carrington, M. E. et al. Sol-gel processing of a covalent organic framework for the generation of hierarchically porous monolithic adsorbents. *Chem* **8**, 2961–2977 (2022).
7. Ascherl, L. et al. Perylene-based covalent organic frameworks for acid vapor sensing. *J. Am. Chem. Soc.* **141**, 15693–15699 (2019).
8. Yang, S. Z. et al. Covalent organic frameworks with irreversible linkages via reductive cyclization of imines. *J. Am. Chem. Soc.* **144**, 9827–9835 (2022).
9. Huang, S. F. et al. Carbazolylene-ethynylene macrocycle based conductive covalent organic frameworks. *Angew. Chem. Int. Ed.* **62**, e202303538 (2023).
10. Kang, C. J. et al. Covalent organic framework atropisomers with multiple gas-triggered structural flexibilities. *Nat. Mater.* **22**, 636–643 (2023).
11. Zhao, W. et al. Using sound to synthesize covalent organic frameworks in water. *Nat. Synth.* **1**, 87–95 (2022).
12. Xu, G. R. et al. Metal organic framework (MOF)-based micro/nanoscaled materials for heavy metal ions removal: The cutting-edge study on designs, synthesis, and applications. *Coordin. Chem. Rev.* **427**, 213554 (2021).
13. Wang, H. et al. Porous two -dimensional materials for photocatalytic and electrocatalytic applications. *Matter* **2**, 1377–1413 (2020).
14. Xu, X. Y. et al. Pore partition in two-dimensional covalent organic frameworks. *Nat. Commun.* **14**, 3360 (2023).
15. Zhu, Y. H. et al. Construction of interlayer conjugated links in 2D covalent organic frameworks via topological polymerization. *J. Am. Chem. Soc.* **143**, 7897–7902 (2021).
16. Yang, S. Z., Streater, D., Fiankor, C., Zhang, J. & Huang, J. E. Conjugation- and aggregation-directed design of covalent organic frameworks as white-light-emitting diodes. *J. Am. Chem. Soc.* **143**, 1061–1068 (2021).
17. Li, Y., Sui, J. F., Cui, L. S. & Jiang, H. L. Hydrogen bonding regulated flexibility and disorder in hydrazone- linked covalent organic frameworks. *J. Am. Chem. Soc.* **145**, 1359–1366 (2023).
18. Feriante, C. H. et al. Rapid synthesis of high surface area imine-linked 2D covalent organic frameworks by avoiding pore collapse during isolation. *Adv. Mater.* **32**, 1905776 (2020).
19. Sick, T. et al. Switching on and off interlayer correlations and porosity in 2D covalent organic frameworks. *J. Am. Chem. Soc.* **141**, 12570–12581 (2019).
20. Kang, C. J. et al. Tunable interlayer shifting in two-dimensional covalent organic frameworks triggered by CO2 sorption. *J. Am. Chem. Soc.* **144**, 20363–20371 (2022).
21. Kang, C. J. et al. Aggregated structures of two-dimensional covalent organic frameworks. *J. Am. Chem. Soc.* **144**, 3192–3199 (2022).
22. Kang, C. J. et al. Interlayer shifting in two-dimensional covalent organic frameworks. *J. Am. Chem. Soc.* **142**, 12995–13002 (2020).

23. Feriante, C. et al. New Mechanistic Insights into the Formation of Imine-Linked Two-Dimensional Covalent Organic Frameworks. *J. Am. Chem. Soc.* **142**, 18637–18644 (2020).
24. Ascherl, L. et al. Molecular docking sites designed for the generation of highly crystalline covalent organic frameworks. *Nat. Chem.* **8**, 310–316 (2016).
25. He, Y. J. et al. Multiple heteroatom-hydrogen bonds bridging electron transport in covalent organic framework-based supramolecular system for photoreduction of CO. *Angew. Chem. Int. Ed.* **62**, e202307160 (2023).
26. Zhao, C. F. et al. Urea-linked covalent organic frameworks. *J. Am. Chem. Soc.* **140**, 16438–16441 (2018).
27. Nelson, A. P., Farha, O. K., Mulfort, K. L. & Hupp, J. T. Supercritical processing as a route to high internal surface areas and permanent microporosity in metal-organic framework materials. *J. Am. Chem. Soc.* **131**, 458–460 (2009).
28. Canham, L. T. et al. Luminescent anodized silicon aerocrystal networks prepared by supercritical drying. *Nature* **368**, 133–135 (1994).
29. Peng, L. et al. Preserving porosity of mesoporous metal-organic frameworks through the introduction of polymer guests. *J. Am. Chem. Soc.* **141**, 12397–12405 (2019).
30. Le Ouay, B., Kitagawa, S. & Uemura, T. Opening of an accessible microporosity in an otherwise nonporous metal-organic framework by polymeric guests. *J. Am. Chem. Soc.* **139**, 7886–7892 (2017).
31. Iizuka, T., Honjo, K. & Uemura, T. Enhanced mechanical properties of a metal-organic framework by polymer insertion. *Chem. Commun.* **55**, 691–694 (2019).
32. Kang, C. J. et al. Growing single crystals of two-dimensional covalent organic frameworks enabled by intermediate tracing study. *Nat. Commun.* **13**, 1370 (2022).
33. Xue, T. W. et al. Green Synthesis of Robust Imine-Linked Two-Dimensional Covalent Organic Frameworks in Supercritical Carbon Dioxide. *Chem. Mater.* **34**, 10584–10593 (2022).
34. Wu, X. L. et al. Packaging and delivering enzymes by amorphous metal-organic frameworks. *Nat. Commun.* **10**, 5165 (2019).
35. Mondloch, J. E., Karagiaridi, O., Farha, O. K. & Hupp, J. T. Activation of metal-organic framework materials. *CrystEngComm* **15**, 9258–9264 (2013).
36. Xie, C. J. et al. Macroscopic-scale preparation of aramid nanofiber aerogel by modified freezing- drying method. *ACS Nano* **15**, 10000–10009 (2021).
37. Zhao, S. Y., Malfait, W. J., Guerrero-Alburquerque, N., Koebel, M. M. & Nyström, G. Biopolymer aerogels and foams: chemistry, properties, and applications. *Angew. Chem. Int. Ed.* **57**, 7580–7608 (2018).
38. Abelenda, A. M. & Dolny, P. Production of ammonium bicarbonate from the condensate of the upgrading biogas-pipelines. *J. Clean. Prod.* **449**, 141787 (2024).
39. Abelenda, A. M. Isolation of ammonium bicarbonate by reactive distillation of food waste digestate liquor. *Bioresource Technol* **399**, 130592 (2024).
40. Xue, T.W. et al. Preserving high porosity of covalent organic frameworks via functional polymer guest introduction. *J. Am. Chem. Soc.* https://doi.org/10.1021/jacs.4c10273 (2024).
41. Neumann, C. et al. Bottom-up synthesis of graphene monolayers with tunable crystallinity and porosity. *ACS Nano* **13**, 7310–7322 (2019).
42. Kohl, I. et al. Raman spectroscopic Study of the phase transition of amorphous to crystalline beta-carbonic acid. *Angew. Chem. Int. Ed.* **48**, 2690–2694 (2009).
43. Sun, D. T., Gasilova, N., Yang, S. L., Oveisi, E. & Queen, W. L. Rapid, selective extraction of trace amounts of gold from complex water mixtures with a metal-organic framework (MOF)/polymer composite. *J. Am. Chem. Soc.* **140**, 16697–16703 (2018).
44. Yu, D. X. et al. Boosting Zn and NH storage in aqueous media via in-situ electrochemical induced VS /VO heterostructures. *Adv. Funct. Mater.* **31**, 2008743 (2021).
45. Cao, L. M., Zhang, J., Zhang, X. F. & He, C. T. Confinement synthesis in porous molecule-based materials: a new opportunity for ultrafine nanostructures. *Chem. Sci.* **13**, 1569–1593 (2022).
46. Xiong, H., Wang, H. Q., Chen, X. & Wei, F. Atomic imaging of zeolites and confined single molecules by iDPC-STEM. *ACS Catal* **13**, 12213–12226 (2023).
47. Sui, R. H. & Charpentier, P. Synthesis of metal oxide nanostructures by direct sol-gel chemistry in supercritical fluids. *Chem. Rev.* **112**, 3057–3082 (2012).
48. Meng, D. et al. Covalent organic frameworks editing for efficient metallaphotoredox catalytic carbon-oxygen cross coupling of aryl halides with alcohols. *Catal Sci Technol* **13**, 1518–1526 (2023).
49. Miao, Z. et al. A novel strategy for the construction of covalent organic frameworks from nonporous covalent organic polymers. *Angew. Chem. Int. Ed.* **58**, 4906–4910 (2019).
50. Das, P., Chakraborty, G., Tyagi, S. & Mandal, S. K. Design of fluorescent and robust covalent organic framework host matrices for Illuminating mechanistic insight into solvatochromic decoding. *ACS Appl. Mater. Interfaces* **12**, 52527–52537 (2020).
51. Flanders, N. C. et al. Large exciton diffusion coefficients in two-dimensional covalent organic frameworks with different domain sizes revealed by ultrafast exciton dynamics. *J. Am. Chem. Soc.* **142**, 14957–14965 (2020).
52. Liu, T. et al. Ordered macro-microporous single crystals of covalent organic frameworks with efficient sorption of iodine. *J. Am. Chem. Soc.* **145**, 2544–2552 (2023).
53. Xie, Y. Q. et al. Ionic functionalization of multivariate covalent organic frameworks to achieve an exceptionally high iodine-capture capacity. *Angew. Chem. Int. Ed.* **60**, 22432–22440 (2021).
54. Scheringer, M. Innovate beyond PFAS. *Science* **381**, 251–251 (2023).
55. Trang, B. et al. Low-temperature mineralization of perfluorocarboxylic acids. *Science* **377**, 839–845 (2022).
56. Ateia, M., Alsbaiee, A., Karanfil, T. & Dichtel, W. Efficient PFAS removal by amine-functionalized sorbents: critical review of the current literature. *Environ. Sci. Tech. Let.* **6**, 688–695 (2019).
57. Wang, W. et al. Preparation of magnetic covalent triazine frameworks by ball milling for efficient removal of PFOS and PFOA substitutes from water. *Environ. Sci. Nano* **9**, 1466–1475 (2022).
58. Wang, W., Zhou, S. X., Jiang, X. Z., Yu, G. & Deng, S. B. Fluorinated quaternary ammonium covalent organic frameworks for selective and efficient removal of typical per- and polyfluoroalkyl substances. *Chem. Eng. J.* **474**, 145629 (2023).

Acknowledgements

L.P. acknowledges funding support from the National Natural Science Foundation of China (grant no. 22373080, 21903066) and President Fund of Xiamen University (grant no. 20720210046). J.L. acknowledges funding support from the National Natural Science Foundation of China (grant no. 22078274). S.Y. acknowledges funding support from the Fundamental Research Funds for the Central Universities (grant no. 20720240054). H.J. acknowledges funding support from the National Natural Science Foundation of China (grant no. 22331009, 22101269). The authors gratefully thank Zeyu Shao, Yanyin Wu, Hongtao Wang, Yuzhong Su and Yanzhen Hong for helpful experiments and discussions.

Author contributions

H.J., L.P., J.L. and S.Y. proposed the research direction and guided the project. T.X. designed and per-formed the experiments. C.L., R.L., R.Q. and S.S. helped with the experiments and characterizations. T.X., L.P., S.Y., G.X., J.L., H.J. and L.Z. analyzed and discussed the experimental results and drafted the paper. Y.Q. and X.G. joined the discussion of the data and gave helpful suggestions. All authors contributed to the writing of the paper.

Competing interests

The authors declare no competing interests.

Additional information

Supplementary information The online version contains supplementary material available at https://doi.org/10.1038/s41467-025-57311-w.

Correspondence and requests for materials should be addressed to Li Peng, Shuliang Yang, Jun Li or Hai-Long Jiang.

Peer review information *Nature Communications* thanks the anonymous, reviewer(s) for their contribution to the peer review of this work. A peer review file is available.